JTTEE5 23:514–524
DOI: 10.1007/s11666-013-0049-y
1059-9630/$19.00 © ASM International

Microstructural Evolution of 6061 Aluminum Gas-Atomized Powder and High-Pressure Cold-Sprayed Deposition

M. R. Rokni, C. A. Widener, and V. R. Champagne

(Submitted July 22, 2013; in revised form September 30, 2013)

Gas-atomized 6061 aluminum powder was used as feedstock for deposition using a high pressure cold-spraying process. The microstructures of the as-received powder and cold spray processed (CSP) ultrafine-grained (UFG) 6061 depositions were characterized by different electron microscopy techniques. It was found that there is segregation of solute elements at the particle grain boundaries, which is increased after cold spraying (CS). Various microstructural features were observed in both directions (parallel and perpendicular) of the CSP layer, including low-angle grain boundaries, clustered-small-cell walls, and dislocation tangle zones. The results also indicated that a combination of different recrystallization mechanisms (i.e., continuous and geometrical) may contribute to the formation of nano and UFG structures during CS.

Keywords aluminium, cold spraying, electron microscopy, microstructure, recrystallization

1. Introduction

Cold gas dynamic spraying or CS is a unique solid-state materials consolidation process that utilizes high velocity particles impinging upon a substrate to build up coatings and/or freestanding structures without the use of combustion fuels. The inherent advantages of this process, which have been previously described in the literature (Ref 1-4), make it a serious competitor for deposition of nanocrystalline metallic materials. Furthermore, in contrast to conventional cold working methods, such as cold rolling, torsion and compression, CS imposes much higher strains into the lattice to generate UFG microstructures. In this process, solid particles smaller than 50 μm reach velocities ranging normally from 500 to 1000 m/s, which leads to strains up to about 10 (corresponding to strain rates of 10^6/s to 5×10^9/s), and fabricate dense coatings with UFG size range (0.1-1 μm) (Ref 4-11). In general, both types of interfaces involved in this process (particle/substrate interface and particle/particle interface) can be strongly affected by heterogeneous strains and strain rates experienced during impact (Ref 6-12). The particle/substrate interface has been studied extensively in recent years (Ref 1, 8-11), but much less attention has been dedicated to the particle/particle interface and how the particles interact with each other during CS.

In the last decade, many metals and alloys, including Al and its alloys, Cu, Ni, and its alloys, and steels, have been successfully processed by the CS technique. Non-uniform microstructures in these deposits have been studied by different electron microscopes interesting features like high dislocation density regions, geometric necessary boundaries (GNBs), pancake-like shaped grains surrounded by well-defined high angle boundaries (HAGBs), elongated subgrains, ultrafine grains with heavy strain contrast near the bonding regions have been characterized (Ref 5-7 & 12-17). Similar features have been previously reported in the microstructures of some of the other severe plastic deformation (SPD) techniques, such as such as laser deposition and cold rolling (Ref 18-20). These microstructural features are the result of higher imposed strains during cold spray processing, which may create an excess amount of inhomogeneously distributed dislocations in some regions, and/or restoration processes, like recrystallization and recovery. However, due to the lack of appropriate results and the limited examined areas of transmission electron microscopy (TEM), the relationship between these features and the powder microstructure, and the main mechanism of their formation have not been well described in the literature.

In UFG materials the fraction of grain boundaries is much larger than in conventional coarse-grained alloys. Non-equilibrium grain boundaries (non-equilibrium GBs) have been the most controversial microstructural feature in nanostructured materials processed by SPD techniques (Ref 21-25). Valiev et al (Ref 21) defined it as a GB that holds extrinsic dislocations that are not needed to

M.R. Rokni and **C.A. Widener**, Department of Materials & Metallurgical Engineering, Advanced Materials Processing Center, South Dakota School of Mines & Technology (SDSM&T), Rapid, SD; and **V.R. Champagne**, U.S. Army Research Laboratory, Weapons and Materials Research Directorate, Aberdeen Proving Ground, Aberdeen, MD. Contact e-mail: mohammadreza.rokni@mines.sdsmt.edu.

accommodate the misorientation across the GB. But no attention has been paid to the correlation between dislocation structure and pile up in cold spraying and non-equilibrium GB formation in the related microstructures. Therefore, it has been the target of this research and is discussed based on the observations made by TEM.

The main objective of this work is to study the microstructural features and dislocation structures in nanostructured 6061 deposited layer processed by CS. The secondary aim is to investigate the main grain refinement mechanisms through TEM observations of dislocations structures and to elucidate the existence of non-equilibrium GBs produced by cold spraying.

2. Experimental procedure

2.1 Cold Spray Processing

In the present study, a 6061 coating was produced using a commercially available gas-atomized 6061 Al powder with an average size of 38.7 μm (measured with a Microtrac S3000 instrument) as the feedstock. Fig. 1 shows the microstructure of the feedstock powder in which spherical shape and size range of particles can be seen. It was observed that the particle size was relatively uniform, consisting of good mixture of larger and smaller particles, but a limited number of micro-satellite sized particles (i.e., less than 5 μm).

Helium was used as the process gas to achieve high impact between incident particles. The deposits were made using a high-pressure CGT 4000 cold spray system and the pressure and temperature of helium were maintained at 2.8 MPa and 400°C at the heater exit, respectively. The deposit was made to a total thickness of 10 mm.

2.2 Microstructural Evaluation

The microstructure of the as-received powder and CSP 6061 aluminum alloy deposited layer was evaluated by high resolution TEM (HRTEM), TEM and the corresponding selected area patterns (SADP), X-ray diffraction (XRD) technique, Dispersive X-ray spectroscopy (EDX) analysis, scanning electron microscopy (SEM). TEM micrographs and the corresponding SADPs were obtained by utilizing a JEM-2100 LaB_6 equipped with Energy Dispersive X-ray spectroscopy (EDX) analysis operating at 200 kV. Thin discs of 3 mm diameter were excised from different directions of the deposition, and then polished, dimpled, and ion milled for 4 hours. TEM analysis for the as-received powder involved suspending Al powders in acetone, ultrasonicating for 10 min, dipping a copper grid into the solution, drying for 10 min and inserting into a vacuum chamber for an hour before inserting the sample into the TEM chamber. The XRD patterns were recorded on the as-received powder and the CS deposited layer. The XRD experiment was performed by a D8 Bruker diffractometer with negligible instrumental broadening using Cu $K\alpha_1$ radiation in the range 2θ = 35-105 using a step size of 0.02 and a counting time of 1s per step. The powder morphology and the deposition microstructure were examined using a Zeiss Supra 40VP SEM. Prior to SEM observations, the deposition samples were sectioned from two different directions perpendicular and parallel to the particle impact vector (Y and Z) and were prepared by standard metallographic techniques.

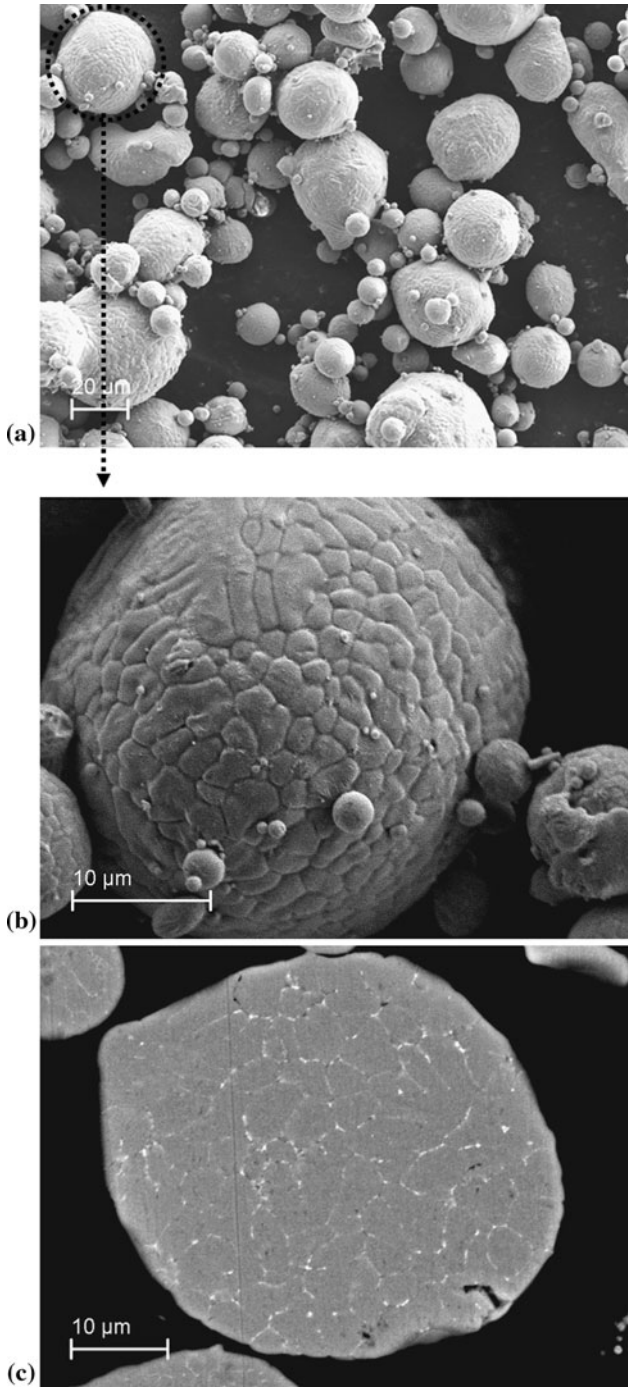

Fig. 1 SEM images from the as-received 6061 Al powder showing (a) powder morphology, (b) Surface grain structure of the powder, (c) GBs solutes segregation in powder particles

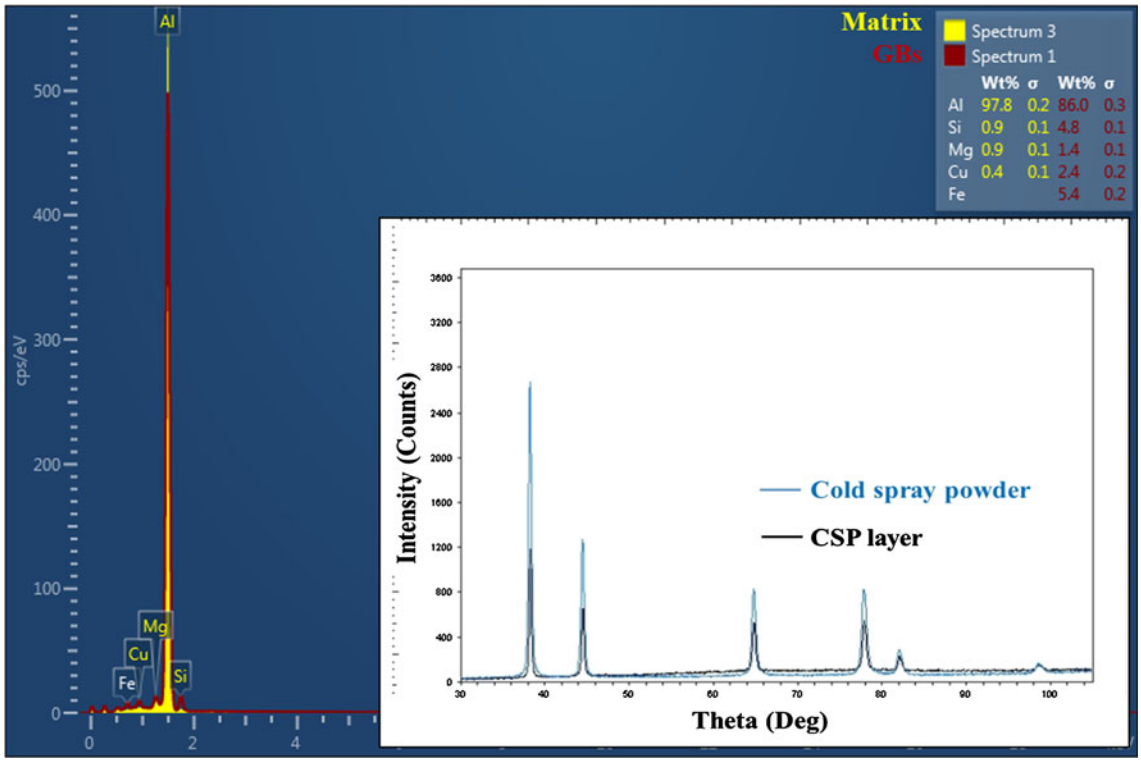

Fig. 2 The EDS analysis comparison between of the as-atomized 6061 powder GB and matrix, and inserted XRD pattern for the powder and as-sprayed deposition

3. Results and discussion

3.1 As-received 6061 Al powder

Fig. 1(a), clearly depicts a typical crystallite particle size in the range of ~ 35 μm for the as-received 6061 Al powder particle. The circled particle in Fig. 1(a) is seen in Fig. 1(b) in which the grain structure of the as-received powder can be observed. According to the image scale, the powder structure consists of grains in the range of 1-4 μm. The back-scattered SEM image in Fig. 1(c) illustrates that the same grain structure is presented inside of the powder particles as well. As can be seen in this figure, the GBs have different chemical compositions compared with the matrix, which is evidence of solutes segregation in the particles. The EDS analysis of the as-atomized 6061 powder shows (Fig. 2) that the GBs in the powder particles are rich in Si, Mg, Cu and Fe elements. This solute segregation can be related to the nature of the powder producing procedure. Since atomized powder is produced by very high solidification rates from liquid temperatures, but does not necessarily cool quickly below the solidus temperature, retained heat in the particles collected after solidification could allow for the solute elements to diffuse to the GBs. In the inserted XRD pattern only FCC Al reflection peaks, with a distinct shift from the pure FCC Al peaks toward lower diffraction angles, were observed. The lattice parameter of the solid solution is ~0.4088 nm, which is notably larger than that of pure Al (0.4050 nm), which can be attributed to the dissolved Mg and Si atoms. According to the inserted XRD pattern there is no lattice parameter difference between the as-received powder and the as-sprayed deposited material, since there is no peak position variation before and after the cold spray processing.

Figure 3a elicits that the starting powder grains are not relaxed and there is some stress inside these powders, and therefore they possess high and uniform dislocation densities (DD). The inserted SADP shows a net pattern, which indicates that the area has some low misorientations. As a result, the grain structure consists mainly of nearly equiaxed subgrains, which might be associated with well-defined substructures and even UFG structures after the cold spray processing (Ref 6, 7, 26, 27). The presence of the equiaxed subgrains and dislocations structures were also proven by an EBSD study of the powder particles. As can be seen in Fig. 3(b), most of the grains in the particle have interior low angle GBs (LAGBs), which in some grains with higher DD converted to the substructure and subgrains.

3.2 Cold Sprayed Layer Microstructure

3.2.1 SEM observations. High magnification SEM images of the CSP layer (Fig. 4), show the rigid and stressed but smooth structure of the 6061 Al coating in the two different directions. In the *Z* direction the grain structure is deformed normal to the impact direction,

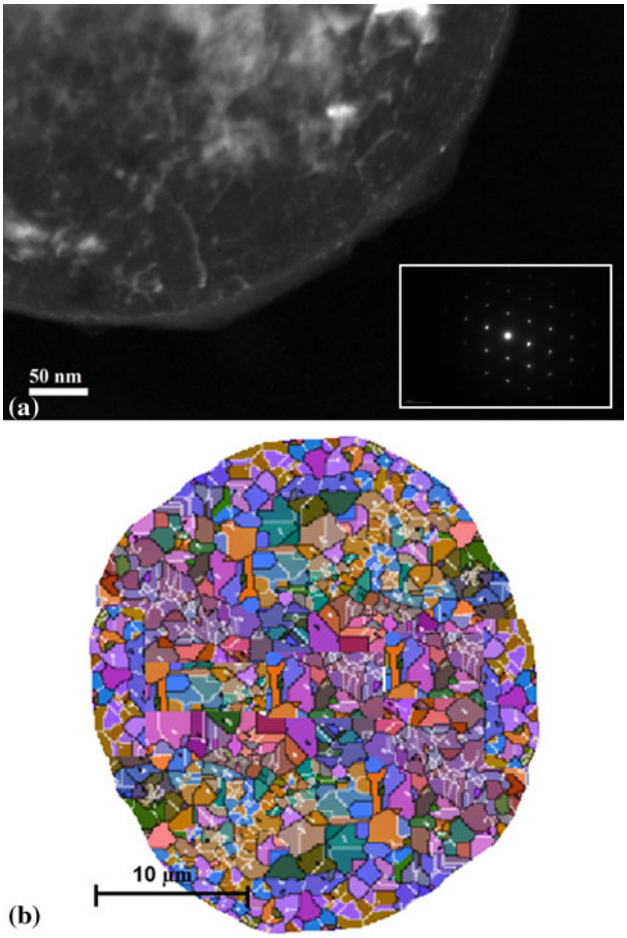

Fig. 3 (a) TEM dark-field image showing the presence of dislocations and substructure (inserted SADP showing net pattern) and (b) EBSD image showing the interior grain structure and LAGBs in the powder microstructure

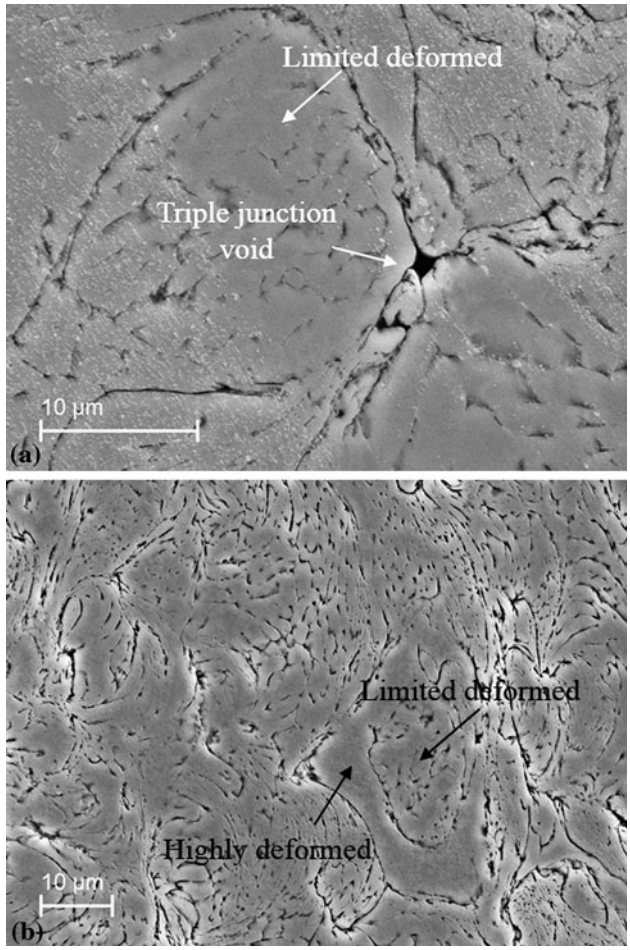

Fig. 4 High magnification SEM images of the CSP 6061 deposition from (a) *Z* direction showing the presence of triple junction void, (b) *Y* direction showing overall deformation in different regions

while in the *Y* direction, the material has been squeezed between two previously deposited splats, resulting in a compression of the grain structure.

As is indicated in Fig. 4(a) there is some evidence of triple junction voids in the deposited layer, which may cause lower ductility in the *Z* direction. These voids generally form via the lack of local deformation in the particles caused by the nature of the coating process (Ref 28). The main reason for the presence of these occasional voids in the microstructure of the *Z* direction can be related to the ''critical'' impact velocity (CIV). The CIV can be defined, as that which results in adequate consolidation of the particles and can be determined by the predictive models developed by ARL (Ref 2). This value is different for large particles and they are not able to achieve the predicted CIV, as such would not completely deform during impact. This also occurs since the particle velocity is a function of the particles location in the gas stream. As such, the process generally involves a degree of randomness in both the particle acceleration kinetics and the particle and substrate interaction, i.e. the variations in the substrate geometries as the deposition builds up. Furthermore, the high velocity-impacts of the spray powders cause very high strain rates, and the large number of particles in flight can cause interactions between particles either before or even during impact. Finally, deposited highly strained particles may be impacted immediately by other particles straight away following the deposition of the next layer of powder. This limited relaxation time after the deposition, in turn, can cause high strain hardening and consequently higher hardness in the deposited coating. Taken together, these factors easily explain the random voids observed within the structure of the cold spray deposit.

On the other hand, abrupt local deformation in a limited period experienced by the powders in *Y* direction generated higher jet flow or adiabatic shear instability and condensation of the sprayed structure resulting in less and smaller triple junction boundaries, which can be seen in Fig. 4(b). The adiabatic regime during the particle impact can lead to thermal softening that would facilitate the plastic deformation and interlocking of splats, allowing each particle to conformably shape to the previous layer

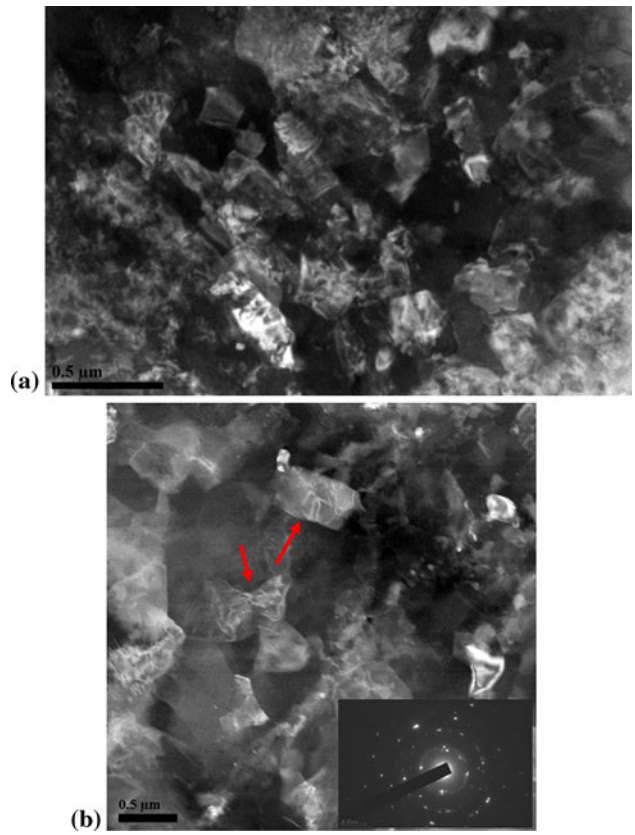

Fig. 5 TEM images from the 6061 deposited layer showing individuals grains their size range. (a) Heavily strained grains with high dislocation density inside. (b) STEM image showing the presence of subgrains and dislocation structure inside of some of the grains. Inserted SADP indicates polycrystalline structure

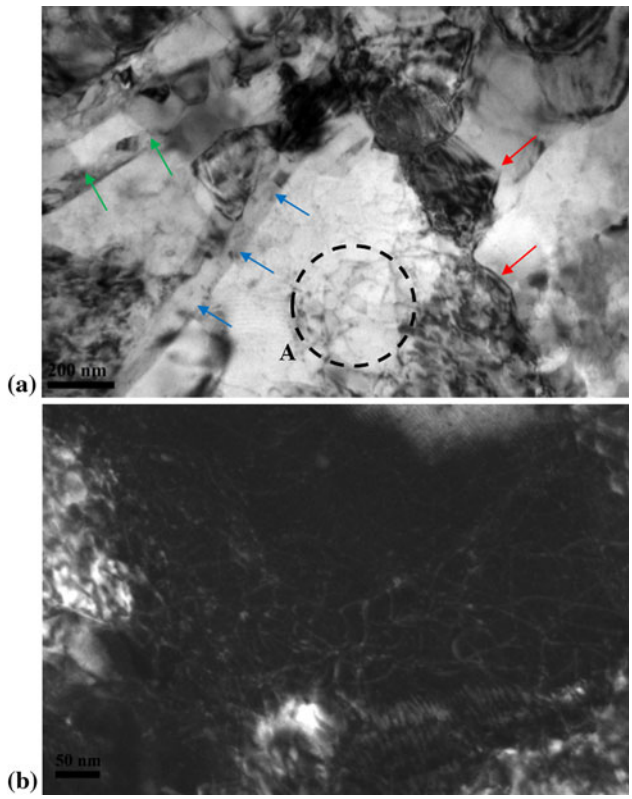

Fig. 6 TEM images from the CSP deposition. (a) *Bright-field* image in which different microstructural features shown with *colored arrows*. (b) *Dark-field* image from the circled area showing high dislocation density in the deposited layer

producing a dense coating. Figure 4(b) also shows evidence of higher overall plastic deformation in this direction. As shown, for many grains the level of deformation varies from the leading edge, which is heavily deformed, to the back of the splat which shows little or limited deformation. Intense shear localization at particle/particle boundaries (highly deformed areas) causes the spherical particles being deformed into long thin splats. However, slight changes to the aspect ratio (width /height) of the particle were observed in the limited deformed regions. This leads to bimodal grain structure in the CSP layer. Because of the highly deformed microstructure in the particle/particle interface, plastic deformation, creating true metallurgical bonding from recrystallization at the interface, and interlocking of splats appears to be the main bonding mechanisms in the CSP 6061 layer.

3.2.2 TEM Observations. Figure 5(a) is a TEM micrograph showing that the individual grains were produced with the sizes ranging from the UFG range of a few hundred nanometers down to the nanoscale with grains less than 100 nm, separated by HAGBs. Some grains are heavily strained and contain a high density of dislocations. As shown with red arrows in Fig. 5(b), some of the grains have ~50 nm interior subgrains, or dislocation structures, which means they have undergone different levels of recovery during CS. The corresponding inserted SADP in Fig. 5(b) exhibits diffraction rings, indicating a polycrystalline structure. The spreading of spots in the diffraction pattern and the contrast variations inside the grains in the scanning TEM (STEM) images point to a significant level of internal stress, crystal lattice distortions, and the presence of very small microstructural features along the high angle grain boundaries resulting from CS. They are usually attributed to a high dislocation density at the grain boundaries associated with their high energy and long-range internal stresses (Ref 29). It has also been well established that these dislocations can act as diffusion paths for solute atoms, and provide nucleation sites for precipitation during processing and post-heat treatment, respectively, which will be discussed in the following sections.

3.2.3 Microstructural Features in the *Z* Direction. Figure 6 shows TEM images from the microstructure in the *Z* direction after CS. The high-velocity impact of the powders caused high plastic deformation and resulted in high dislocation density, as well as recovery and crystallization after the cold spraying in certain regions. As indicated in Fig. 6(a), the deformation is clearly inhomogeneous, as shown by the mixture of equiaxed and pancaked grains, dislocation cell structure, subgrains, dislocation-tangle zones (DTZs) and microbands (MBs). This can be explained by the effect of strain rate

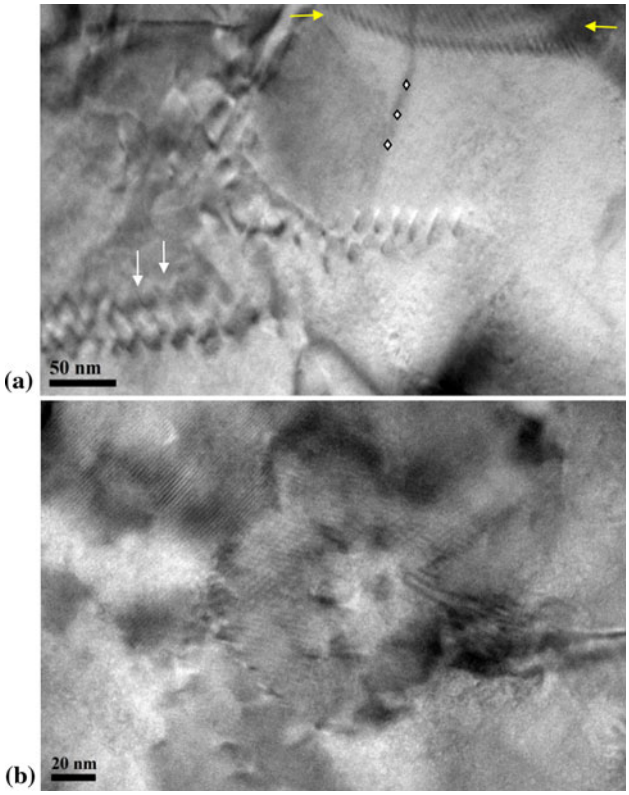

Fig. 7 TEM images from the 6061 CSP deposition showing the presence of (a) LAGBs and substructure and (b) dislocation loops in the microstructure

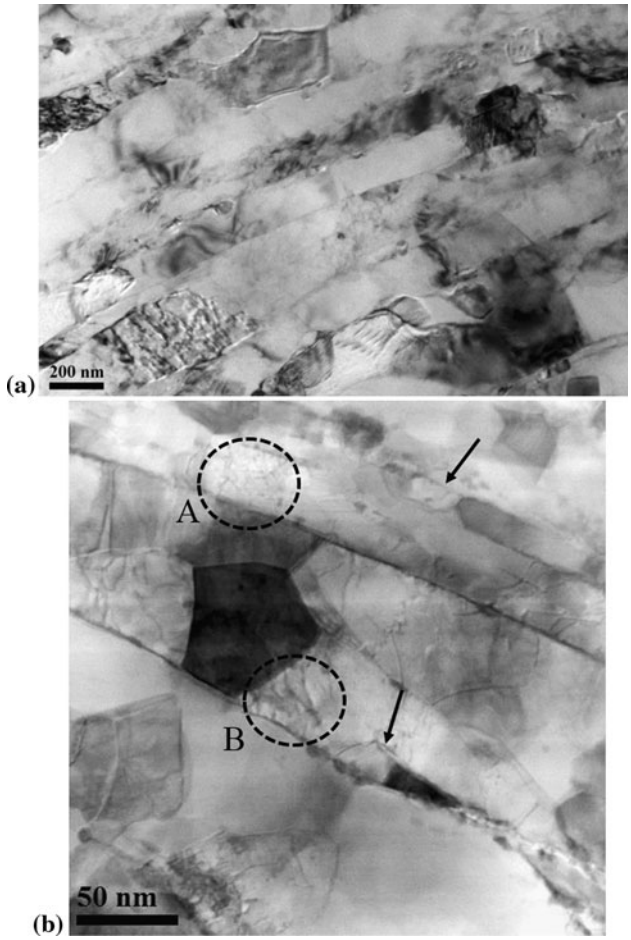

Fig. 8 TEM images from the 6061 CSed layer in *Y* direction showing (a) lamellar MBs and elongated microstructure, (b) presence of subgrains inside of some MBs

on slip system activity and lattice rotation. Since higher strain rates promote lattice rotation in simple shear to a greater extent than lower strain rates, then there must be a mixture of low and high angle boundaries between the adjacent grains on the interfacial particle areas (Ref 6, 7, 14, 29).

Dislocation cell structure was also observed in subgrains in some areas, like region A in Fig. 6(a), which can be also called clustered-small-cell walls (CSCWs) (Ref 29, 30). The cell boundaries are incidental dislocation boundaries (IDBs) that form by trapping glide dislocations (Ref 18, 31, 32). Some IDBs at large strains may develop a higher misorientation and become geometric GNBs, which integrate into the lamellar structure and act like LAGBs which interconnect with the lamellar boundaries. Also as indicated in Fig. 6(a) (green arrows), we do observe low angle interconnecting boundaries in the 6061 CSP layer microstructure. These cells may also form individual subgrains upon further plastic straining.

We frequently observed dislocation tangles in the interior of the grains, as marked by red arrows in Fig. 6(a), where the grain is heavily strained and called a DTZ. During CS, even in the same grains or subgrain, slip systems will change when the accumulative strain is very high, which can lead to more interaction of dislocations with each other and consequently can result in the formation of DTZs (Ref 29).

HRTEM image in Fig. 7(a) shows the separation of a subgrain by a dense-sliding dislocation wall (DDW) (marked by yellow arrows in Fig. 7(a)) and the generation of a grain interface are both found in some grains and subgrains in the microstructure. Several other fine features can be observed in the interior of the subgrains. As indicated by two yellow arrows in the same figure, a high density of extrinsic dislocations is piled up along the (111) plane to make a non-equilibrium subgrain boundary. Using the HRTEM image, glissile dislocations were observable mostly along the {111} planes producing about 7° of misorientation between these two subgrains. A LAGB was also characterized in this grain, as marked by diamonds in Fig. 7(a). The LAGB was also formed by the accumulation of a number of glissile dislocations. Figure 7(b) shows a HRTEM image from a highly strained grain in the microstructure. The presence of dislocation loops in the microstructure is deducible from this image. In this case, the dislocation loops are believed to be primarily agglomerations of interstitials and vacancies formed during or immediately after the cold spray process (Ref 5). Because of restrictions of tilting in the electron

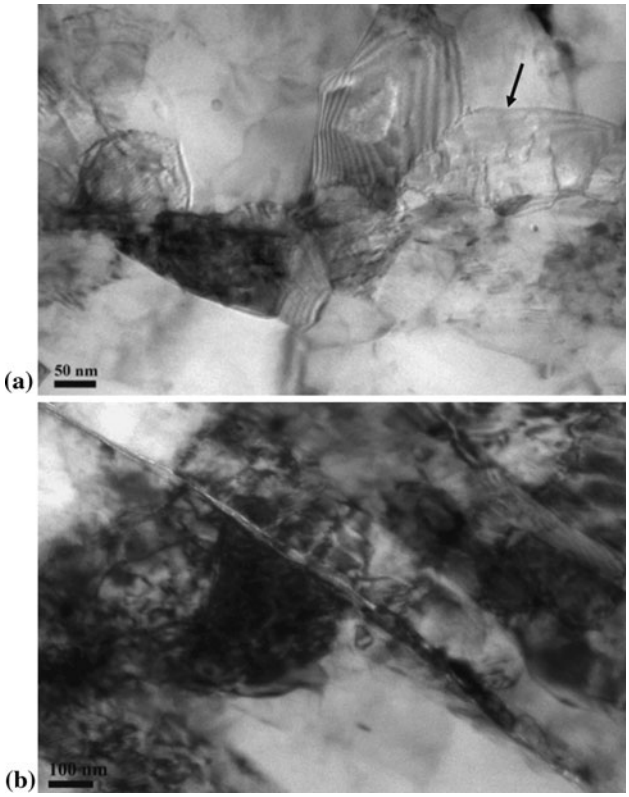

Fig. 9 TEM images from the 6061 CSed deposition in *Y* direction showing (a) array of dislocations piled on a particular plane of subgrains and (b) absorption of dislocations into subgrain and MB boundaries

microscope, it is not possible to determine unambiguously the exact Burgers vectors and habit planes of the loops.

As mentioned in Sect. 3.2.1, good particle/particle bonds in the as-deposited microstructure can be attributed to a higher degree of deformation, which is further related to adiabatic shear instabilities occurring at the particle/particle interface during cold spraying. Thus, it can be concluded the higher degree of bonding observed between particles is related to the greater deformation seen in these high pressure deposits. Furthermore, the high deformations also facilitate the conversion of high-energy dislocations into nano grains, subgrains, forming interfaces and MBs that are composed of small pancake-shaped cells (SPCs, blue arrows in Fig. 6(a)). Regardless of whether the particles remain equiaxed or are heavily deformed, these shear instabilities at the particle/particle interface cause a large number of ultrafine grains in the size of 20-200 nm.

3.2.4 Microstructural Features in the *Y* Direction. The TEM micrographs of the CSP layer in the *Y* direction (perpendicular to deposition direction) are seen in Fig. 8. Figure 8(a) shows lamellar MBs with well-defined grain boundaries and interior elongated nano grains. The formation of MBs results from crystallographic slip on a dominant slip system and then propagation through multiple- or cross-slip events because of a stress concentration, accompanied with the production of a large amount of dislocations between the slip planes (Ref 6). Kikuchi analysis revealed that nearly all of the lamellar boundaries were high angle in character and they thus delineate long thin-ribbon-shaped grains. The grains can be seen to extend across the entire figure and contain transverse LAGBs with a spacing of 50-200 nm (Fig. 8a, b), producing a ''ladder-like'', or ''bamboo'', structure.

Dislocation substructures were also observed in this direction inside some of the MBs as well as dislocation cells that were separated by DDWs. In regions with more stored energy, DDWs were annihilated and replaced by subgrains with clear boundaries (black arrow in Fig. 9a), which are mostly composed of dislocation arrays piled on a particular plane (Ref 20-22). The combination of dislocation free grains, subgrains, DTZs, and SPCs can be observed in Fig. 9(a), which signifies the deformation is inhomogeneous in this direction, similar to the *Z* direction.

Figure 8(b) also shows CSCWs (region A) formed by some uncondensed dislocation walls (UDWs) which can subsequently transform into small dislocation cells or subgrains, as seen in region B. Dislocations generated during deformation in CS are absorbed into the UDWs and increase their misorientation until they transform into LAGBs (Ref 6, 13, 33). As shown in Fig. 9(b), it was also observed that the absorption of dislocations into subgrain and MB boundaries was sufficient enough to build very thick grain boundaries in certain places.

3.2.5 Nano and UFG Structure Formation Mechanism. In aluminum alloys with high-stacking fault energy, the dynamic recovery (DRV) and dynamic recrystallization (DRX) may take place upon deformation at high temperatures (Ref 10, 11). These alloys, due to the high efficiency of dynamic recovery and the low mobility of their grain boundaries, are more prone to the continuous DRX (CDRX) than to the discontinuous DRX (DDRX).

Figure 10 shows EBSD images of the CSP layer in the *Z* direction. The particle-particle interactions caused the formation of nano grains at the interfaces of highly deformed particles (Fig. 10a). Although the formation mechanism of the nano grains during high strain induced plastic deformation is still an issue under discussion, preceding investigations suggest that the formation process of such grains is based on a nano CDRX mechanism (Ref 6, 30, 33). During CDRX, the development of the recrystallized microstructure is occurred through progressive transformation of the subgrains into the new grains. In accordance with previous published results (Ref 6, 8, 13), the most possible mechanism for CDRX in the microstructure is subgrain rotation, which can be explained as follows.

As soon as the impact occurs, dislocations are propagated and form substructure and DTZ. As discussed previously, Fig. 5(a) and (b) is evidence of substructure formation and DTZ during CS processing. As indicated with black rectangles in Fig. 10(b), due to the large number of dislocations accumulated and aligned at extremely high strain rates, elongated UFG structures were formed. These grains were subdivided into equiaxed subgrains due to the increased dislocation density. In

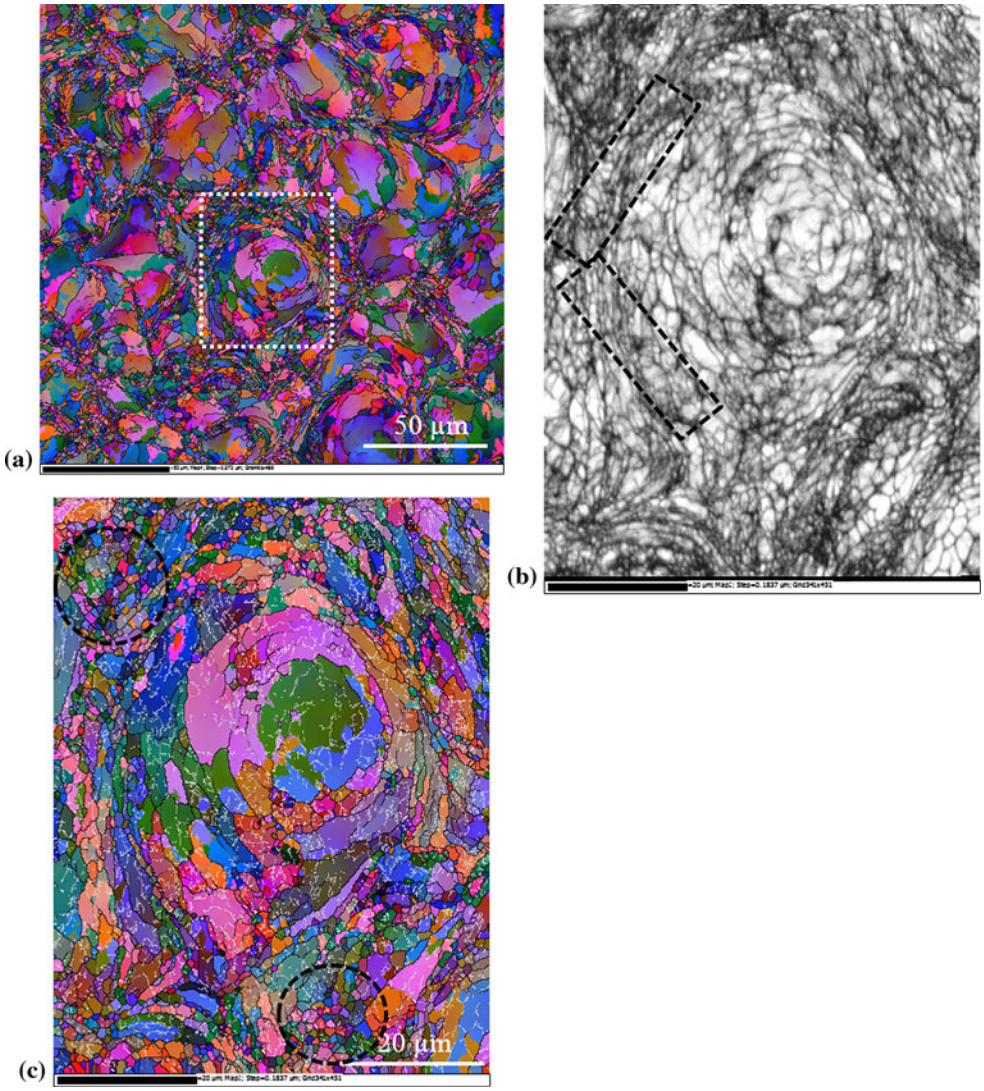

Fig. 10 EBSD images from the CSP 6061 deposition in *Z* direction, (a) particle/particle interaction in the deposit, (b) and (c) Euler angle map and pattern quality map showing the presence of the UFG structures at the particle/particle interface and LAGBs and subgrains throughout the microstructure

zones with sufficient deformation, the misorientations between adjacent subgrains increased enough that LAGBs fully transformed into HAGBs, forming nano grains, as seen in Figs. 6(a) and 8(a). In case where there is not enough deformation to convert, LAGBs remain in the microstructure as a substructure even after CS, as seen in Fig. 10(c).

The formation of some of the nano and UFG structure regions (white circles in Fig. 10c) could also be a characteristic feature of geometric dynamic recrystallization (GDRX) (Ref 34-37). This is easily understood, since the deformation and processing heat creating during CS can cause some of the grains to experience a temperature in the range of the recovery process. The latter results in the formation of developed serrations at the grain boundaries, which with the processing of the next layer can turn into some nano-equiaxed grains. This kind of microstructure is more evident in the *Y* direction. As shown in Fig. 11, the recrystallized zones associated with the interaction and collision of different particles can be clearly seen, which would also be in agreement with a GDRX mechanism for generating UFG structure in this direction. Figure 11(b) and (c) is higher magnification micrographs from the dashed rectangular area in Fig. 11(a). Figure 11(b) shows substructure and dislocation structures (white lines) which are common features throughout the microstructure. One point that should not be excluded here is that the grain structure observed in the as-received powder (Sect. 3.1) can also contribute to the formation of some nano-sized and UFG structure by GDRX.

Finally, the presence of nano scale precipitates throughout the microstructure and at GBs in both the *Z* and *Y* directions, was also observed (Fig. 12). By comparing the EDS analysis of the as-received powder and

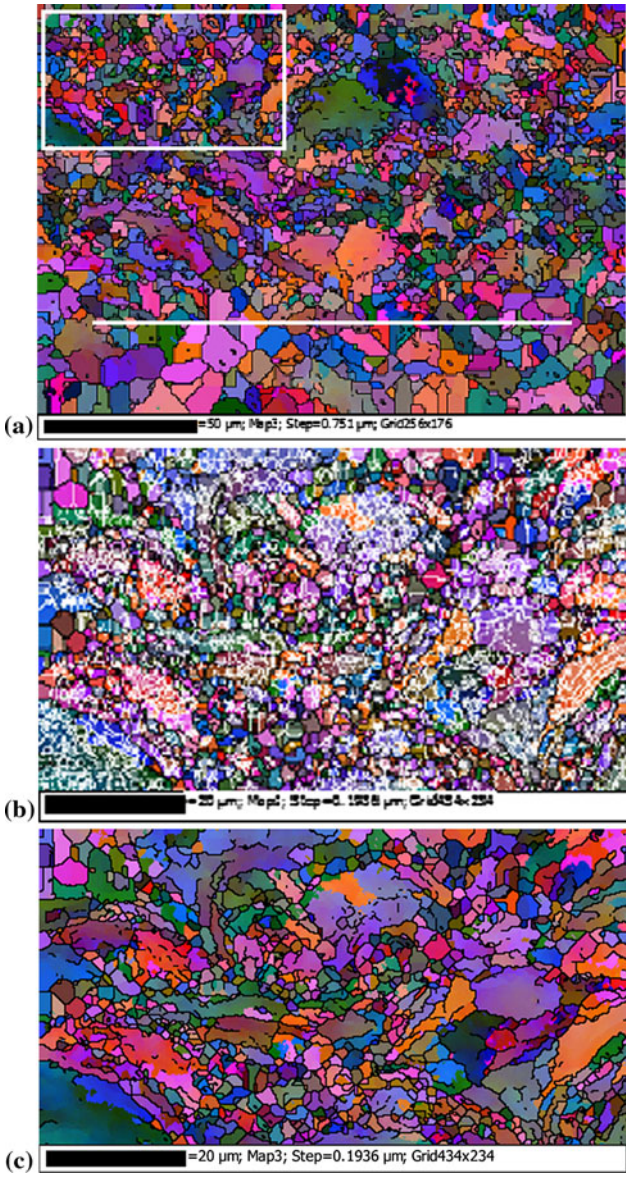

Fig. 11 EBSD images from the CSP 6061 deposition in *Y* direction, (a) particles interaction in the deposit, (b) and (c) Euler angle map and pattern quality map showing the presence of the UFG structures at the particle/particle interface and LAGBs and subgrains throughout the microstructure

CSP deposition, it was evident that these are Cu-, Si-, Mg-, and Fe-rich precipitates that have nucleated during the CS process. This is significant, since it has been well established that the presence of high densities of precipitates at GBs and within the grains in aluminum alloys act as effective obstacles to dislocation movement and hence may cause DD differences between the two sides of a boundary. For areas which experience recovery temperatures, boundary migration during CS is likely to happen and the resultant difference in DD may also result in recrystallization by strain induced boundary migration (SIBM) (Ref 33). But while this assumption is quite

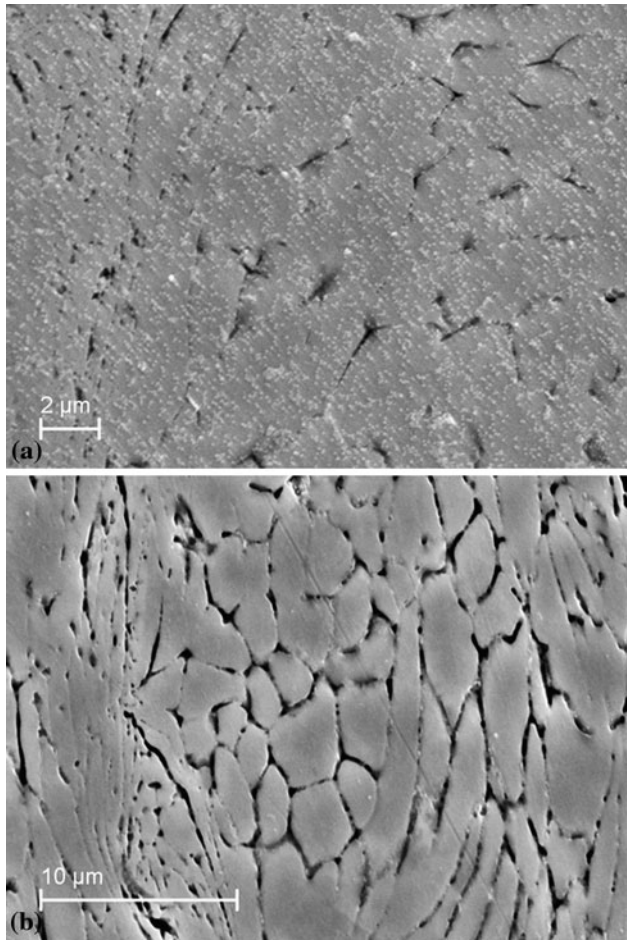

Fig. 12 SEM images from the CSP 6061 deposition, (a) presence of nano scale precipitates throughout the microstructure in *Z* direction and (b) precipitates at the GBs in *Y* direction

interesting, a more detailed investigation would need to be conducted before drawing any reliable conclusions. For now, it suffices to say that in the high pressure CSP 6061 layer, the combination of different recrystallization mechanisms (CDRX, GDRX and SIBM) contributes to the formation of new nano and UFG recrystallized zones.

4. Conclusions

Microstructural evolution in a CSP 6061 layer was investigated via different electron microscopy techniques (TEM, HRTEM, EBSD, and SEM). Several important conclusions resulted from this work. First, based on the highly dense UFG 6061 aluminum alloy coatings observed here, CS can be a promising new technique for producing bulk nanostructured metal materials. Second, various microstructural features (i.e., including LAGBs, CSCWs, DTZs) were observed in both directions (parallel and perpendicular) of the CSP layer. Next, the resulting CSP layer was highly influenced by the microstructure of the

initial powder, and those structures could be found preserved or contributing to the state of transformed structures. Finally, it was observed that the pancaked microstructure and particle/particle interfaces contain UFG and nanosize recrystallized grains evolving from microbands formed under the high strain rates of CS. Evidence for two main formation mechanisms for the observed microstructural features using TEM, HRTEM and EBSD were presented, namely CDRX and GDRX.

Acknowledgements

This study was performed under subcontract to the Pueblo Economic Development Corporation (PEDCO) under Army Research Lab contract no. W911NF-11-2-0014.

References

1. W.B. Choi, L. Li, V. Luzin, R.A. Neiser, T. Gnaupel-Herold, H.J. Prask, S. Sampath, and A. Gouldstone, Integrated Characterization of Cold Sprayed Aluminum Coatings, *Acta Mater.*, 2007, **55**, p 857-866
2. V.K. Champagne, *The Cold Spray Materials Deposition Process: Fundamentals and Applications*, Woodhead Publishing Limited, Cambridge, 2007
3. R.C. Dykhuizen, M.F. Smith, D.J. Gilmore, R.A. Neiser, X. Jiang, and S. Sampath, Impact of High Velocity Cold Spray Particles, *J. Thermal Spray Technol.*, 1999, **4**, p 559-564
4. Phani P. Sudharshan, V. Vishnukanthan, and G. Sundararajan, Effect of Heat Treatment on Properties of Cold Sprayed Nanocrystalline Copper Alumina Coatings, *Acta Mater.*, 2007, **55**, p 4741-4751
5. C. Borchers, F. Gärtner, T. Stoltenhoff, and H. Kreye, Formation of Persistent Dislocation Loops by Ultra-High Strain-Rate Deformation During Cold Spraying, *Acta Mater.*, 2005, **53**, p 2991-3000
6. Y. Zou, W. Qin, E. Irissou, J.G. Legoux, S. Yue, and J.A. Szpunar, Dynamic Recrystallization in the Particle/Particle Interfacial Region of Cold-Sprayed Nickel Coating: Electron Backscatter Diffraction Characterization, *Scr. Mater.*, 2009, **61**, p 899-902
7. Y. Zou, D. Goldbaum, J.A. Szpunar, and S. Yue, Microstructure and Nanohardness of Cold-Sprayed Coatings: Electron Backscattered Diffraction and Nanoindentation Studies, *Scr. Mater.*, 2010, **62**, p 395-398
8. H. Assadi, F. Gärtner, T. Stoltenhoff, and H. Kreye, Bonding Mechanism in Cold Gas Spraying, *Acta Mater.*, 2003, **51**, p 4379-4394
9. G. Bae, Y. Xiong, S. Kumar, K. Kang, and C. Lee, General Aspects of Interface Bonding in Kinetic Sprayed Coatings, *Acta Mater.*, 2008, **56**, p 4858-4868
10. K. Kim, M. Watanabe, J. Kawakita, and S. Kuroda, Grain Refinement in a Single Titanium Powder Particle Impacted at High Velocity, *Scr. Mater.*, 2008, **59**, p 768-771
11. T. Schmidt, F. Gärtner, H. Assadi, and H. Kreye, Development of a Generalized Parameter Window for Cold Spray Deposition, *Acta mater.*, 2006, **54**, p 729-742
12. X. Wang, J. Zhao, and J. He, Investigation on the Microstructure and Mechanical Properties of the Spray-Formed Cu-Cr Alloys, *Mater. Sci. Eng. A*, 2007, **460-461**, p 69-76
13. S.R. Bakshi, V. Singh, K. Balani, D.G. McCartney, S. Seal, and A. Agarwal, Carbon Nanotube Reinforced Aluminum Composite Coating via Cold Spraying, *Surf. Coat. Tech.*, 2008, **202**, p 5162-5169
14. Q. Wang, N. Birbilis, and M.X. Zhang, Interfacial Structure Between Particles in an Aluminum Deposit Produced by Cold Spray, *Mater. Lett.*, 2011, **65**, p 1576-1578
15. P.D. Eason, J.A. Fewkes, S.C. Kennett, T.J. Eden, K. Tello, M.J. Kaufman, and M. Tiryakioglu, On the Characterization of Bulk Copper Produced by Cold Gas Dynamic Spray Processing in the As-Fabricated and Annealed Conditions, *Mater. Sci. Eng. A*, 2001, **528**, p 8174-8178
16. T.H. Van Steenkiste and J.R. Smith, Evaluation of Coatings Produced via Kinetic and Cold Spray Processes, *J. Thermal Spray Technol.*, 2004, **13**, p 274-282
17. Y.Y. Zhang and J.S. Zhang, Recrystallization in the Particles Interfacial Region of the Cold-Sprayed Aluminum Coating: Strain-Induced Boundary Migration, *Mater. Lett.*, 2011, **65**, p 1856-1858
18. Q. Liu, X. Huang, D.J. Lloyd, and N. Hansen, Microstructure and Strength of Commercial Purity Aluminium (AA 1200) Cold-Rolled to Large Strains, *Acta Mater.*, 2002, **50**, p 3789-3802
19. R. Lupoi, M. Sparkes, A. Cockburn, and W. O'Neill, High Speed Titanium Coatings by Supersonic Laser Deposition, *Mater. Lett.*, 2011, **65**, p 3205-3207
20. R.Z. Valiev, R.K. Islamgaliev, and I.V. Alexandrov, Bulk Nanostructured Materials from Severe Plastic Deformation, *Mater. Sci.*, 2000, **45**, p 103-189
21. R.Z. Valiev, Y. Gertsman, and O.A. Kaibyshev, Grain Boundary Structure and Properties Under External Influences, *Phys. Status Solidi. A*, 1986, **97**, p 11-56
22. R.Z. Valiev, O.A. Kaibyshev, and S.K. Khnnanov, Grain Boundaries During Superplastic Deformation, *Phys. Status Solidi. A*, 1979, **52**, p 447-453
23. A.A. Nazarov, A.E. Romanov, and R.Z. Valiev, On the Structure, Stress Fields and Energy of Nonequilibrium Grain Boundaries, *Acta Metall.*, 1993, **41**, p 1033-1040
24. S. Ferrase, V.M. Segal, K.T. Hartwig, and R.E. Goforth, Microstructure and Properties of Copper and Aluminum Alloy 3003 Heavily Worked by Equal Channel Angular Extrusion, *Metall. Mater. Trans.*, 1997, **28A**, p 1047-1057
25. Z. Horita, D.J. Smith, M. Furukawa, M. Nemoto, R.Z. Valiev, and T.G. Langdon, An Investigation of Grain Boundaries in Submicrometer-Grained Al-Mg Solid Solution Alloys Using High-Resolution Electron Microscopy, *J. Mater. Res.*, 1996, **11**, p 1880-1890
26. G.R. Canova, C. Fressengeas, A. Molinari, and U.F. Kocks, Effect of Rate Sensitivity on Slip System Activity and Lattice Rotation, *Acta Metall.*, 1988, **36**, p 1961-1970
27. M.R. Rokni, A. Zarei-Hanzaki, H.R. Abedi, and N. Haghdadi, Microstructure Evolution and Mechanical Properties of Backward Thixoextruded 7075 Aluminum Alloy, *Mater. Des.*, 2012, **36**, p 557-563
28. G.E. Dieter, *Mechanical Metallurgy*, McGraw-Hill Series in Materials Science and Engineering McGraw-Hill, Singapore, 2001
29. J.Y. Huang, Y.T. Zhu, H. Jiang, and T.C. Lowe, Microstructures and Dislocation Configurations in Nanostructured Cu Processed by Repetitive Corrugation and Straightening, *Acta Mater.*, 2001, **49**, p 1497-1505
30. B. Bay, N. Hansen, D.A. Hughes, and D. Kuhlmann-Wilsdorf, Overview no. 96 Evolution of fcc Deformation Structures in Polyslip, *Acta Mater.*, 1992, **40**, p 205-219
31. D.A. Hughes, N. Hansen, and D.J. Bammann, Geometrically Necessary Boundaries, Incidental Dislocation Boundaries and Geometrically Necessary Dislocations, *Scr. Mater.*, 2003, **48**, p 147-153
32. Q. Liu and N. Hansen, Geometrically Necessary Boundaries and Incidental Dislocation Boundaries Formed During Cold Deformation, *Scr. Metal. Mater.*, 1995, **32**, p 1289-1295
33. M.E. Kassner and S.R. Barrabes, New Developments in Geometric Dynamic Recrystallization, *Mater. Sci. Eng. A*, 2005, **410-411**, p 152-155
34. F.J. Humphreys and M. Hatherly, *Recrystallization and Related Annealing Phenomena*, 2nd ed., Pergamon Press, Oxford, 2004
35. M.R. Rokni, A. Zarei-Hanzaki, and H.R. Abedi, Microstructure Evolution and Mechanical Properties of Back Extruded 7075 Aluminum Alloy at Elevated Temperatures, *Mater. Sci. Eng. A*, 2012, **532**, p 593-600

36. M.R. Rokni, A. Zarei-Hanzaki, A.A. Roostaei, and H.R. Abedi, An Investigation into the Hot Deformation Characteristics of 7075 Aluminum Alloy, *Mater. Des.*, 2011, **32**, p 2339-2344

37. W. Blum, Q. Zhu, R. Merkel, and H.J. McQueen, Geometric Dynamic Recrystallization in Hot Torsion of Al-5Mg-0.6Mn (AA5083), *Mater. Sci. Eng. A*, 1996, **205**, p 23-30